World Scientific
www.worldscientific.com

EFFECTS OF SHOCK PRESSURE AND SELF-GENERATED ELECTRIC FIELD ON SHOCK-INDUCED FERROELECTRIC TO ANTIFERROELECTRIC PHASE TRANSITION IN LEAD ZIRCONATE STANNATE TITANATE FERROELECTRIC CERAMICS

DONGDONG JIANG* and YUJUN FENG

Electronic Materials Research Laboratory
Xi'an Jiaotong University, Xi'an 710049, P. R. China
and
International Center for Dielectric Research
Xi'an Jiaotong University, Xi'an 710049, P. R. China
*jiangdongeast@163.com

JINMEI DU and YAN GU

National Key Laboratory of Shock Wave and Detonation Physics
Institute of Fluid Physics, CAEP, Mianyang 621900, P. R. China

Kinetics of the ferroelectric (FE) to antiferroelectric (AFE) phase transformation under shock wave compression is critical to design the shock-activated power supply and can be characterized in terms of both a transition rate and a limiting degree of transition. By measuring the depoling currents under the short-circuit and high-impedance conditions, we investigated the influence of shock pressure and self-generated electric field on the phase transition kinetics of tin-modified lead zirconate titanate ceramics $(Pb_{0.99}Nb_{0.02}[(Zr_{0.90}Sn_{0.10})_{0.96}Ti_{0.04}]_{0.98}O_3)$ in the pressure range from 0.23 to 4.50 GPa. Experimental results indicate that the shock pressure promotes the FE-to-AFE phase transition. And the self-generated electric field does not appear to have a significant effect on the depoling currents at high shock pressures, but has a strong effect at low pressures. At 0.61 GPa and 1.03 GPa, transition rate and degree diminish with increasing the electric field, illustrating that the self-generated electric field suppresses the FE-to-AFE phase transition. These observations are found to be generally consistent with results under the hydrostatic compression. Fundamental issues are discussed from the perspective of the soft mode theory.

Keywords: Shock wave; ferroelectric; antiferroelectric; phase transition.

1. Introduction

A ferroelectric (FE) is a material with spontaneous electrical polarization that can be reoriented by an applied electric field.[1] Closely related to the FE is the antiferroelectric (AFE), which also possesses polarization with antiparallel orientation so that no macroscopic polarization can rise.[2] Free-energy difference between the FE and AFE states is very small for composition close to the FE/AFE phase boundary. Thus, it is easy to induce the FE/AFE phase transition on application of a suitable temperature,[3,4] electric field,[5,6] and pressure.[7,8] These phase transitions are usually accompanied by a volume expansion/contraction,[9] a development/release of electrical polarization,[10] or an incommensurate modulation in structure,[11−14] having many engineering applications. For instance, pressure-induced phase switching involves the release of a large electrical polarization, which is useful in conversion of mechanical to electrical energy and is an area of great current interest in a broad range of functional ferroelectric materials.[15−17]

Recently, rapid depolarization associated with the shock wave induced FE-to-AFE phase transition has attracted considerable attention, because of the application of the shock-activated power supply.[18−24] The kinetics of the FE-to-AFE phase transformation under the shock wave compression is characterized in terms of both a transition rate and a limiting degree of transition.[25] In the shock wave loading, the depoling current associated with the depolarization flows through the resistive load and generates electric field (E) between the electrodes. Under the short-circuit condition (resistive load $R = 0$, $E = 0$), effect of the shock pressure on the transition rate and degree have been investigated by Setchell and Montgomery.[25] Under the high-impedance condition ($E > 0$), effect of the self-generated electric field on the rate and degree of the phase transition is still unknown. Compared with the short-circuit case, we are more interested in the kinetics of the FE-to-AFE phase transition under the high-field condition. The reason is that the released energy ω is $\varepsilon_0\varepsilon_r E^2/2$, where ε_0 is the dielectric constant of free space, ε_r is the relative dielectric constant. To obtain a large energy output, the ceramic has to be subjected to a high electric field. Moreover, how the electric field modifies the phase transition kinetics also is a critical question in the shock-activated power supply from an application viewpoint. Thus, it is important to investigate the influence of the self-generated electric field on the kinetics of the FE-to-AFE phase transition.

In this article, we report the effect of shock pressure and self-generated electric field on the FE-to-AFE phase transformation in the tin-modified lead zirconate titanate ($Pb(Zr,Sn,Ti)O_3$) ceramics under shock wave compression. Attention is paid to the dependence of the transition rate and degree on the shock pressure and the self-generated electric field. Experimental observations are in accordance with the soft-mode theory and the results under the hydrostatic compression.

2. Samples and Experiments

2.1. *Samples*

Tin-modified lead zirconate titanate ferroelectric ceramic was selected and the composition was $Pb_{0.99}Nb_{0.02}[(Zr_{0.90}Sn_{0.10})_{0.96}Ti_{0.04}]_{0.98}O_3$ (PZST). This composition was near the phase boundary between the orthorhombic antiferroelectric (A_O) phase and low-temperature rhombohedral ferroelectric (F_{RLT}) phase. Samples were prepared by conventional solid-state reaction using the reagent-grade raw materials such as Pb_3O_4, ZrO_2, TiO_2, SnO_2, and Nb_2O_5. The sintering process was carried out in a lead-rich environment in order to minimize lead volatilization. At last samples were coated with silver electrodes and poled under an electric field of $3\,KV/mm$ at $100\,°C$ for $5\,min$ in a silicon oil bath. The parameter was as follows: density $\rho_0 = 7.80\,g/cm,^3$ piezoelectric constant $d_{33} = 68.0\,pC/N$, remanent polarization $P_r = 28.0\,\mu C/cm.^2$

2.2. *Shock wave experiments*

The kinetics of the FE-to-AFE phase transformation was investigated by the impact-experiment. Figure 1(a) shows the schematic diagram of the shock wave experiment. 2024 aluminum (Al 2024) projectile body with a flat-surfaced facing was propelled down the barrel of an air gun and impacted onto a flat-surfaced polymethyl methacrylate (PMMA) target facing. The PMMA target face was precisely aligned parallel to the Al 2024 or PMMA projectile facing and perpendicular to the axis of the barrel. The velocity of the projectile at impact (u_0) was obtained by measuring the time interval between velocity pins close to the target facing.
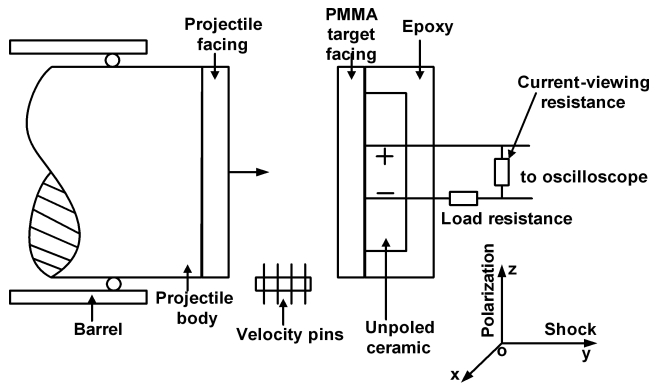
(a)
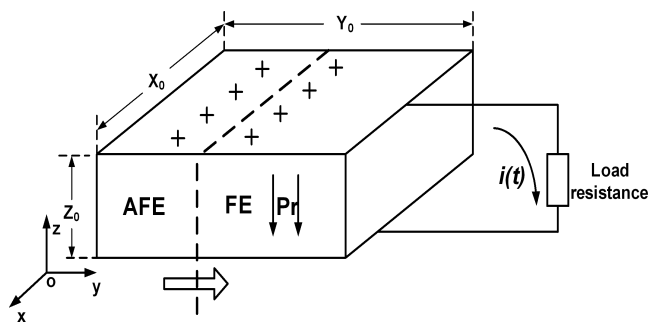
(b)

Fig. 1. (a) Schematic diagram of the shock wave experiments. (b) Shock wave compression of ferroelectric ceramics in normal mode, in which the shock wave vector is perpendicular to the vector of remanent polarization. The shock front is indicated by the dash line.

The impact initiated a shock wave propagating into the PZST ceramics. The dimensions of the PZST ceramics were $X_0 = 30.0$ mm in the x-direction, $Y_0 = 10.0$ mm in the direction of the shock wave and $Z_0 = 2.0$ mm in the direction of the remanent polarization (Fig. 1(b)). Electrodes were deposited on the $X_0 \times Y_0$ faces. So the direction of the shock propagation vector was perpendicular to the remanent polarization. In order to approach a uniaxial strain state, two pieces of unpoled ceramics sandwiched the poled ceramic. The ceramics were encapsulated with epoxy resin to reduce the probability of high-voltage electrical breakdown around their edges.

As the shock wave depolarized the ceramic, the depoling current flowed in the external circuit. The external circuit consisted of a low-inductance load resistance (R) and low-inductance current-viewing resistance (r). In all experiments, r was 1.0 Ω and the voltage appearing on r was transmitted by coaxial cable to an oscilloscope for recording. R was

Table 1. Details of shock wave experiments.

Experiment No.	Projectile facing	Impact velocity u_0 (m/s)	Shock pressure σ_S (GPa)	Load resistance R (Ω)
1	Al 2024	49.6	0.23	200
2	Al 2024	124.2	0.61	200, 300
3	Al 2024	200.6	1.03	200, 300
4	Al 2024	232.3	1.22	200
5	PMMA	473.0	1.60	200
6	Al 2024	424.0	2.47	300
7	PMMA	1073.4	4.50	200

not used under short-circuit condition. Under high-impedance condition, R was put in transformer oil to prevent the dielectric breakdown.

A series of seven shock wave experiments were performed. Table 1 lists the projectile facing, impact velocity, calculated shock pressure and load resistances for each of the experiments. The shock pressure in the PZST ceramic was calculated by using the impedance-match method and dependent on the Hugoniot relations of the Al 2024,[26] PMMA[27] and PZST ceramic. Because the Hugoniot curve of the PZST ceramic had not been determined, the Hugoniot of $Pb_{0.99}Nb_{0.02}(Zr_{0.95}Ti_{0.05})_{0.98}O_3$ (PZT 95/5-2Nb) ceramic (initial density 7.80 g/cm³ was used.[28]

3. Results and Discussion

3.1. *Effects of shock pressure on the FE-to-AFE phase transition*

Figure 2 displays the depoling currents under the short-circuit condition. The self-generated electric field between the electrodes is zero under the short-circuit condition. Two quantities were of considerable importance in any attempt to explain the results. The first quantity was the amplitude. The current was relatively small at 0.23 GPa. As shock pressure increased from 0.61 to 2.47 GPa, the current magnitude increased and reached 22.2 A, 26.5 A, 30.3 A, 31.4 A and 33.7 A, respectively.

The second quantity was the released charge. The released charge obtained by integrating the output currents provides a convenient approach to investigate the evolutionary process of the FE-to-AFE phase transition,[29] which can be better appreciated when the normalized released charge (NRC) with respect to the P_r is plotted as a function of the shock
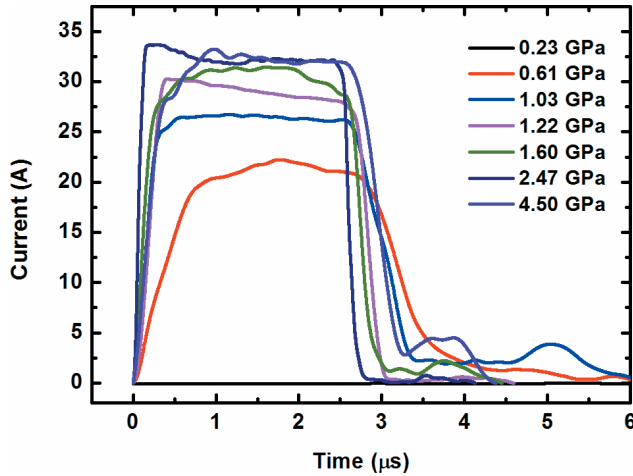
Fig. 2. (Color online) The depoling currents as a function of shock pressure for $Pb_{0.99}Nb_{0.02}[(Zr_{0.90}Sn_{0.10})_{0.96}Ti_{0.04}]_{0.98}O_3$ ceramics under the short-circuit condition.

pressure (Fig. 3). The NRC was given by

$$\text{NRC} = \int_0^{+\infty} I(t)dt/P_r X_0 Y_0. \qquad (1)$$

For comparison, the released charge of PZT 95/5-2Nb ceramics with different density is also shown.[25,30,31] The NRC is close to zero at 0.23 GPa. At 0.61 GPa, NRC is 0.76, indicating that the FE-to-AFE phase transition begins. The released charge increases as the shock pressure increases, demonstrating that more and more FE phase has been transformed into the AFE phase and the shock
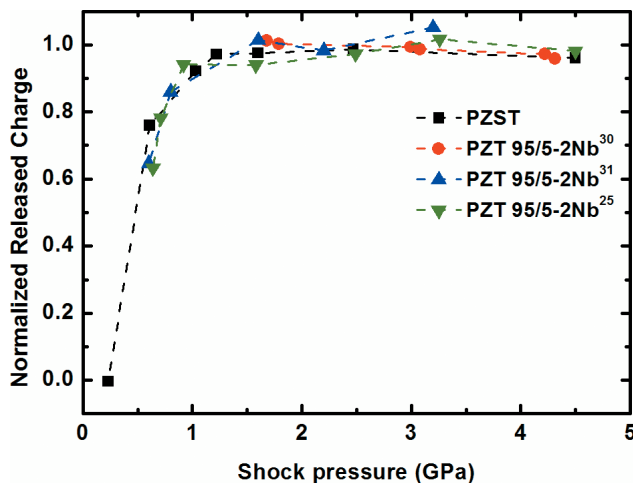

Fig. 3. (Color online) The dependence of the normalized released charge with respect to the P_r on the shock pressure. The P_r is 30.0 $\mu C/cm^2$ for porosity PZT 95/5-2Nb ceramics (7.55 g/cm^3, Ref. 31; 7.30 g/cm^3, Ref. 25) and 32.0 $\mu C/cm^2$ in Ref. 30.

pressure promotes the FE-to-AFE phase transition. Scanning electron microscope (SEM) and transmission electron microscope (TEM) have shown that ferroelectric domains in PZT 95/5-2Nb ceramics become fewer at the higher shock pressure.[32,33] At 1.22 GPa, the NRC is close to 1, indicating the complete liberation of remanent polarization. Thus, by using the criterion of complete liberation of remanent polarization as an indication of the complete phase transformation, the complete transformation pressure is determined to be 1.22 GPa. After the phase transformation is complete, the NRC is insensitive to the shock pressure. Similar dependence of NRC on the shock pressure is also seen in PZT 95/5-2Nb ceramics.

3.2. *Effects of self-generated electric field on the FE-to-AFE phase transition*

3.2.1. *Depoling current*

Figure 4 presents the depoling currents for PZST ceramics as a function of the load resistance in the pressure range from 0.61 to 4.50 GPa. The currents at 0.24 GPa are omitted because of small magnitude. In contrast to the short-circuit cases, strong electric fields are generated between electrodes under the high-impedance condition. One feature that should be noticed is the eventual magnitude. When the shock pressure is strong enough (1.22 GPa, 1.60 GPa, 2.47 GPa and 4.50 GPa), the short-circuit and high-impedance currents have the almost same eventual amplitude. However, the peak current under the high-impedance condition is significantly lower than the peak value under the short-circuit condition at 0.61 GPa and 1.03 GPa. As can be seen in Fig. 3, at 0.61 GPa and 1.03 GPa, the shock wave is not strong enough to complete the phase transition. From the above results, the self-generated electric field does not appear to have a significant effect on the depoling currents at high shock pressures, but has a strong effect at low pressures.

3.2.2. *Kinetics of the FE-to-AFE phase transition*[25,34]

The kinetics is characterized in terms of both a transition rate and a limiting degree of transition and can be directly examined by measuring the depoling current associated with the FE-to-AFE
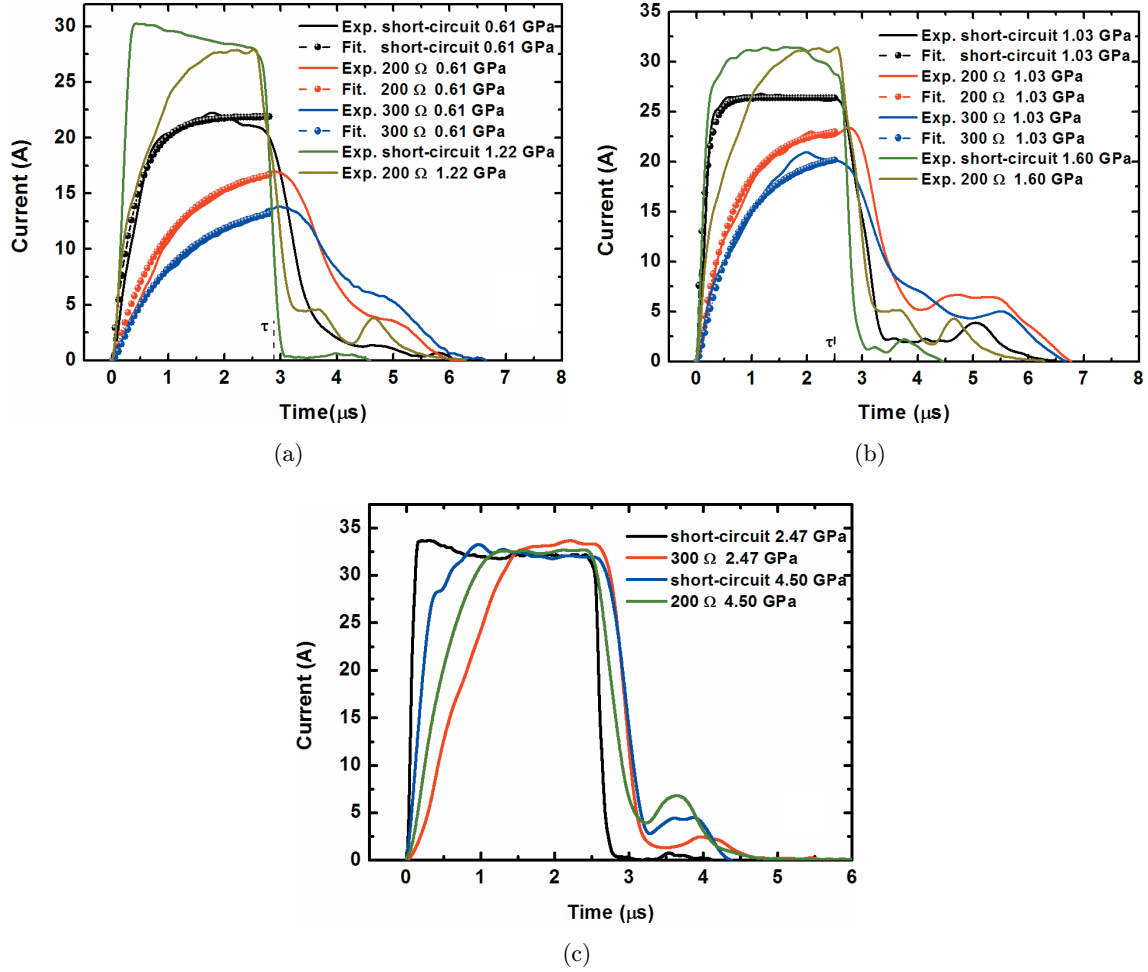
(a)

(b)

(c)

Fig. 4. (Color online) The measured (solid line) and fitted (close circular) depoling currents as a function of load resistance for $Pb_{0.99}Nb_{0.02}[(Zr_{0.90}Sn_{0.10})_{0.96}Ti_{0.04}]_{0.98}O_3$ ceramics at (a) 0.61 GPa and 1.22 GPa, (b) 1.03 GPa and 1.60 GPa, and (c) 2.47 GPa and 4.50 GPa.

phase transition. In Fig. 1(b), at time t, under the short-circuit condition, the depoling current during the shock transient time is expressed as

$$I_{SC} = (P_r - P_{fSC})X_0U_S(1 - \exp(-t/\tau_{SC})),$$
$$t < \tau. \qquad (2)$$

Here, I_{SC} is the short-circuit current, P_r is the remanent polarization, P_{fSC} is the residual polarization behind the shock wave, X_0 and Y_0 are the dimensions of the ceramics, U_S is the velocity of the shock wave, τ_{SC} is the characteristic time for the phase transition, $\tau = Y_0/U_S$ is the shock transition time in ceramic. $1/\tau_{SC}$ is considered as the transition rate and $(P_r - P_{fSC})/P_r$ is the degree of the phase transformation. Increasing the value of $1/\tau_{SC}$ means that phase transition will take place more and more rapidly. The degree is 0 when phase transition does not occur ($P_{fSC} = P_r$); the degree is 100%

when phase transition occurs completely ($P_{fSC} = 0$). Values for τ_{SC} and P_{fSC} can be found from each measured currents by fitting Eq. (2).

The depoling current under the high-impedance ($R > 0$) condition (I_{HP}) is given by

$$I_{HP} = (P_r - P_{fHP})X_0U_S(1 - \exp(-t/\tau_{HP}))$$
$$\cdot (1 - \exp(-t/RC)), \qquad (3)$$
$$t < \tau.$$

Here, P_{fHP} is the residual polarization behind the shock wave, τ_{HP} is the characteristic time, R is the load resistance, and C is the capacity of the ceramic. The self-generated electric field is given by

$$E = I_{HP}R/Z_0, \qquad (4)$$

where Z_0 is the thickness between the electrodes. Under the strong electric field, the capacitance (C) requires that part of the released charge retain on

the electrodes rather than pass through the load resistance. Thus, comparing with the short-circuit cases, the currents with the load resistance increase gradually with the "*RC*" time constant. Similarly, τ_{HP} and $P_{f\mathrm{HP}}$ can be examined from the measured high-impedance currents by fitting Eq. (3). Comparing the differences between $1/\tau_{\mathrm{SC}}$ and $1/\tau_{\mathrm{HP}}$, $(P_r - P_{f\mathrm{SC}})/P_r$ and $(P_r - P_{f\mathrm{HP}})/P_r$, we can investigate the effect of the self-generated electric field on the FE-to-AFE phase transition.

3.2.3. *Results*

We fit the measured short-circuit and high-impedance currents (0.61 GPa and 1.03 GPa) with Eqs. (2) and (3), respectively. Phase transition kinetics in the pressure range from 1.22 to 4.50 GPa are not given because it may be difficult to distinguish between electric field effects on the transition characteristics and the effects of the changing dielectric properties.[34] Table 2 gives the parameters used in the fitting procedure, in which the dielectric property is assumed to be unchanged.[34] The dependence of the transition rate and degree on the peak electric field ($E_{\max} = I_{\max}R/Z_0$) is shown in Fig. 5. Both the transition rate and degree reduce with increasing the electric field for PZST ceramics, demonstrating that phase transition takes place more and more slowly and incompletely under the high field condition. Therefore, it can be concluded that the self-generated electric field retards the phase transition. In contrast, both $1/\tau_{\mathrm{SC}}$ and $(P_r - P_{f\mathrm{SC}})/P_r$ increase with increasing the shock pressure under the short-circuit condition, illustrating that the shock pressure promotes the phase transition.
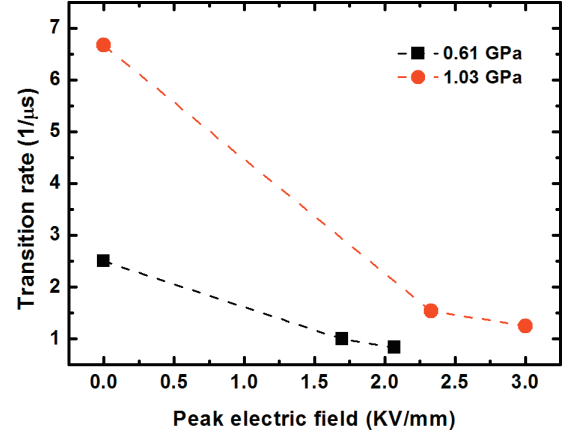
3.3. *Discussion*

We explain the promoting and the suppressing effect from the viewpoint of the soft mode theory. The
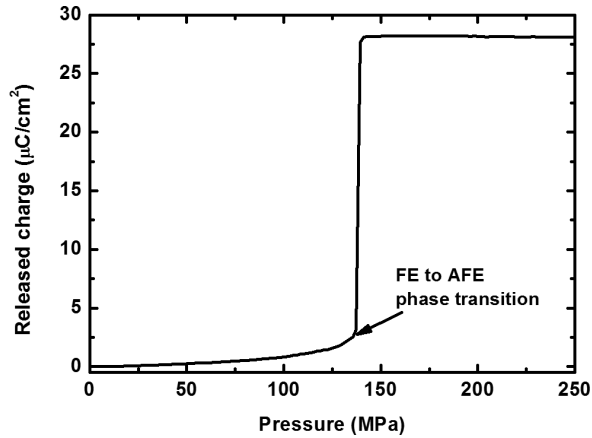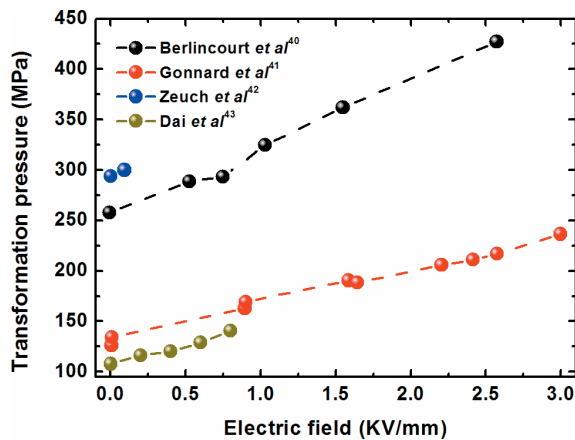

(a)

(b)

Fig. 5. (Color online) The dependence of (a) transition rate and (b) transition degree on the peak self-generated electric field.

concept of a soft mode was proposed by Cochran[35] and confirmed by Baker and Tinkham[36] and Cowley[37] for phase transformations in ferroelectrics. According to the soft-mode theory for phase transformation in ferroelectrics, the FE/AFE phase transformation is determined by the balance of competing forces between the long- and short-range interactions.[38,39] The electric field favors the long-range-ordered FE phase, while the pressure favors the short-range-ordered AFE phase.[39] Thus, under the short-circuit condition, the shock pressure promotes the FE-to-AFE phase transition. Under the high-impedance condition, the presence of the self-generated electric field is especially effective in assisting the long-range ordering FE phase and retards the FE-to-AFE phase transition. Thus, the self-generated electric field is contradictory to the shock pressure. When the shock wave is strong enough (i.e., 1.22−4.50 GPa), although the electric

Table 2. Parameters used in the fitting procedure.

σ_S (GPa)	R (Ω)	ε_r	τ (μs)	U_S (km/s)
0.61	200	308[a]	2.876[b]	3.477
	300	317[a]		
1.03	200	321[a]	2.560[b]	3.906
	300	312[a]		

[a]The dielectric constants were measured by HP4284A LCR meter before shock wave experiments.
[b]See in Figs. 4(a) and 4(b).

(a)

(b)

Fig. 6. (Color online) (a) Hydrostatic pressure induced depolarization of $Pb_{0.99}Nb_{0.02}[(Zr_{0.90}Sn_{0.10})_{0.96}Ti_{0.04}]_{0.98}O_3$ ceramic.[8] (b) The dependence of the FE-to-AFE phase transformation pressure on the biased electric field under the hydrostatic compression for $Pb_{0.99}Nb_{0.02}[(Zr_{0.73}Sn_{0.27})_{0.93}Ti_{0.07}]_{0.98}O_3$ (Ref. 40), $PbZr_{0.95}Ti_{0.05}O_3 + 0.8\%WO_3$ (Ref. 41), $Pb_{0.99}Nb_{0.02}(Zr_{0.95}Ti_{0.05})_{0.98}O_3$ (Ref. 42), and $Pb_{0.99}Nb_{0.02}(Zr_{0.75}Sn_{0.20}Ti_{0.05})_{0.98}O_3$ (Ref. 43) ceramics.

field can also suppress the phase transition, suppressing effect may be weak and hard to be observed.

Similar results are also observed in the hydrostatic experiments. Figure 6(a) illustrates that the hydrostatic pressure induces the FE-to-AFE phase transition for PZST ceramics.[8] The suppressing effect of the biased electric field on the FE-to-AFE phase transition has been observed experimentally by Berlincourt *et al.*[40] in $Pb_{0.99}Nb_{0.02}[(Zr_{0.73}Sn_{0.27})_{0.93}Ti_{0.07}]_{0.98}O_3$, Gonnard *et al.*[41] in $PbZr_{1-x}Ti_xO_3 + 0.8\%WO_3$ $(0.05 \leq x \leq 0.08)$, Zeuch *et al.*[42] in PZT 95/5-2Nb, and Dai *et al.*[43] in

$Pb_{0.99}Nb_{0.02}[Zr_{0.75}Sn_{0.20}Ti_{0.05}]_{0.98}O_3$ ceramics under the hydrostatic compression (Fig. 6(b)). The phase transformation pressure rises with increasing the biased electric field, which illustrates that the electric field can also inhibit the FE-to-AFE phase transition under the hydrostatic compression.

4. Conclusion

Effects of the shock pressure and the self-generated electric field on the FE-to-AFE phase transition under shock wave compression were investigated in PZST ceramics. The shock wave promotes the FE-to-AFE phase transition, exhibiting that transition rate and degree increase with increasing the shock pressure. However, the self-generated electric field retards the FE-to-AFE phase transition, exhibiting that transition rate and degree decrease with increasing the electric field. According to the soft mode theory, the electric field acts to extend the range of stability of the FE state and the compressive stress acts to extend the range of stability of the AFE state. Our experimental results support the argument and are useful in designing the shock-activated power supply.

Acknowledgments

References

1. B. B. Vanaken, T. T. M. Palstra, A. Filippetti and N. A. Spaldin, *Nat. Mater.* **3**, 164 (2004).
2. C. Kittel, *Phys. Rev.* **82**, 729 (1951).
3. J. Frederick, X. Tan and W. Jo, *J. Amer. Ceram. Soc.* **94**, 1149 (2011).
4. D. D. Jiang, Y. J. Feng, H. Tang, Y. Gu and J. M. Du, *Ferroelectrics* **409**, 33 (2010).
5. X. Tan, J. Frederick, C. Ma, E. Aulbach, M. Marsilius, W. Hong, T. Granzow, W. Jo and J. Rödel, *Phys. Rev. B* **81**, 014103 (2010).
6. X. Tan, J. Frederick, C. Ma, W. Jo and J. Rödel, *Phys. Rev. Lett.* **105**, 255702 (2010).
7. M. Avdeev, J. D. Jorgensen, S. Short, G. A. Samara, E. L. Venturini, P. Yang and B. Morosin, *Phys. Rev. B* **73**, 064105 (2006).

8. D. D. Jiang, Y. Gu, Y. J. Feng and J. M. Du, *Acta Phys. Sin.* **60**, 107703 (2011).

9. W. Y. Pan, Q. M. Zhang, A. Bhalla and L. E. Cross, *J. Amer. Ceram. Soc.* **72**, 571 (1989).

10. Z. Xu, Y. J. Feng, S. G. Zheng, A. Jin, F. L. Wang and X. Yao, *J. Appl. Phys.* **92**, 2663 (2002).

11. H. He and X. L. Tan, *Appl. Phys. Lett.* **85**, 3187 (2004).

12. H. He and X. L. Tan, *Phys. Rev. B* **72**, 024102 (2005).

13. H. He and X. L. Tan, *J. Phys.: Condens. Matter* **19**, 136003 (2007).

14. D. Viehland, D. Forst, Z. Xu and J. F. Li, *J. Amer. Ceram. Soc.* **78**, 2101 (1995).

15. D. A. Hall, J. D. S. Evans, S. J. Covey-Crump, R. F. Holloway, E. C. Oliver, T. Mori and P. J. Withers, *Acta Mater.* **58**, 6584 (2010).

16. R. E. Setchell, *J. Appl. Phys.* **94**, 573 (2003).

17. R. E. Setchell, *J. Appl. Phys.* **101**, 053525 (2007).

18. P. C. Lysne and C. M. Percival, *J. Appl. Phys.* **46**, 1519 (1975).

19. J. C. F. Millett, N. K. Bourne and D. Deas, *J. Phys. D: Appl. Phys.* **40**, 2948 (2007).

20. D. D. Jiang, Y. J. Feng, J. M. Du and Y. Gu, *High Pressure Res.* **31**, 436 (2011).

21. D. D. Jiang, J. M. Du, Y. Gu and Y. J. Feng, *J. Phys. D: Appl. Phys.* **45**, 115401 (2012).

22. D. D. Jiang, J. M. Du, Y. Gu and Y. J. Feng, *J. Appl. Phys.* **111**, 104102 (2012).

23. D. D. Jiang, N. Zhang, Y. J. Feng, J. M. Du and Y. Gu, *Mater. Sci. Eng. B* **177**, 210 (2012).

24. D. D. Jiang, J. M. Du, Y. Gu and Y. J. Feng, *Chinese Sci. Bull.* **57**, 2554 (2012).

25. R. E. Setchell, *J. Appl. Phys.* **97**, 013507 (2005).

26. J. M. Walsh, M. H. Rice, R. G. McQueen and F. L. Yarger, *Phys. Rev.* **108**, 196 (1957).

27. L. M. Barker and R. E. Hollenbach, *J. Appl. Phys.* **41**, 4208 (1970).

28. D. G. Doran, *J. Appl. Phys.* **39**, 40 (1968).

29. D. D. Jiang, J. M. Du, Y. Gu and Y. J. Feng, *High Pressure Res.* **32**, 280 (2012).

30. Y. S. Liu, G. M. Liu, F. P. Zhang and H. L. He, *Piezoelect. Acoustoopt.* **30**, 58 (2008).

31. P. C. Lysne, *J. Appl. Phys.* **48**, 1020 (1977).

32. L. C. Chhabildas, Sandia National Laboratories Report SAND84-1729 (1984).

33. L. C. Chhabildas, M. J. Carr, S. C. Kunz and B. Morosin, Sandia National Laboratories Report SAND85-0406C (1985).

34. D. D. Jiang, J. M. Du, Y. Gu and Y. J. Feng, *J. Appl. Phys.* **111**, 024103 (2012).

35. W. Cochran, *Phys. Rev. Lett.* **3**, 412 (1959).

36. A. S. Baker and M. Tinkham, *Phys. Rev.* **125**, 1527 (1962).

37. R. A. Cowley, *Phys. Rev.* **134**, A981 (1964).

38. G. A. Samara, *Phys. Rev. Lett.* **35**, 1767 (1975).

39. P. Yang and D. A. Payne, *J. Appl. Phys.* **80**, 4001 (1996).

40. D. Berlincourt, H. H. A. Krueger and B. Jaffe, *J. Phys. Chem. Solids* **25**, 659 (1964).

41. P. Gonnard, F. Bauer, M. Troccaz, Y. Fetiveau and L. Eyraud, *Appl. Phys.* **3**, 299 (1974).

42. D. H. Zeuch, S. T. Montgomery and D. J. Holcomb, *J. Mater. Res.* **14**, 1814 (1999).

43. Z. Dai, Z. Xu and X. Yao, *Appl. Phys. Lett.* **92**, 072904 (2008).